Eur. Phys. J. D **36**, 57–65 (2005)
DOI: 10.1140/epjd/e2005-00186-5

THE EUROPEAN PHYSICAL JOURNAL D

Accurate characterisation of the C(3)$^1\Sigma^+$ state of the NaRb molecule*

W. Jastrzebski[1], P. Kortyka[1], P. Kowalczyk[2], O. Docenko[3], M. Tamanis[3], R. Ferber[3], A. Pashov[4], H. Knöckel[4,a], and E. Tiemann[4]

[1] Institute of Physics, Polish Academy of Sciences, Al. Lotnikow 32/46 00-668, Warsaw, Poland
[2] Institute of Experimental Physics, Warsaw University, ul. Hoza 69, 00-681, Warsaw, Poland
[3] Department of Physics and Institute of Atomic Physics and Spectroscopy, University of Latvia, 19 Rainis Blvd., 1586 Riga, Latvia
[4] Institut für Quantenoptik, Universität Hannover, Welfengarten 1, 30167 Hannover, Germany

Received 21 December 2004 / Received in final form 2 June 2005
Published online 19 July 2005 –

Abstract. We present a first detailed experimental study of the C(3)$^1\Sigma^+$ state of the NaRb molecule converging to the Na($3p$) + Rb($5s$) states of separated atoms. Two different high resolution spectroscopic methods have been applied: the Fourier transform spectroscopy of laser induced fluorescence and the V-type optical-optical double resonance polarization labeling spectroscopy. The entire data field for the C$^1\Sigma^+$ state of Na^{85}Rb and Na^{87}Rb consists of rovibrational levels with $v' = 0$–64 and $J' = 4$–123. The data were incorporated into a direct fit of a single potential energy curve to the level energies using the Inverted Perturbation Approach method. As the experimental data extend to the "shelf" region of the potential at large internuclear separations of 8.5 Å, the C state's suitability for photoassociation yielding cold heteronuclear NaRb is discussed.

PACS. 31.50.Df Potential energy surfaces for excited electronic states – 32.90.+a Other topics in atomic properties and interactions of atoms with photons (restricted to new topics in section 32) – 33.20.Kf Visible spectra

1 Introduction

Trapping of cold ensembles of mixed species of alkali atoms is a very active topic of research presently. However, only few examples of successful production of cold mixed alkali dimers by photoassociation were reported till now [1–5]. In contrast to the very long range character of excited molecular states of homonuclear alkali dimers, which exhibits the $1/R^3$ form of resonant dipole-dipole interaction, the heteronuclear binding is of the $1/R^6$ type and therefore of much shorter range. As is pointed out in reference [6], nevertheless photoassociation (PA) rates of similar magnitude or only a little bit smaller as compared to e.g. Cs_2 can be expected, provided similar densities in the trapped ensemble can be achieved. On the other hand, it can be helpful to employ excited molecular states which can provide access to larger internuclear separations by some avoided crossing, like double well potentials. In this case it is essential that the electronic transition matrix element does not vanish on going outwards in the nuclear distance through the avoided crossing.

For the electronically excited C$^1\Sigma^+$ state of NaRb the theoretical calculations by Korek et al. [7] predict a shelf in the long range part, which could increase the useful range of nuclear distances for photoassociation. An overview of the lowest Σ and Π electronic states of NaRb is shown in Figure 1. The transition dipole moment function for the C$^1\Sigma^+$–X$^1\Sigma^+$ transition was calculated for internuclear distances from 3 to 7 Å by Zaitsevkii et al. [8] applying the multipartitioning perturbation theory (MPPT). Recently, the transition dipole moment function was calculated also for internuclear separations up to about 15 Å by Aymar and Dulieu [9]. In the interval of internuclear distances which both calculations have in common the values of the dipole moments from both sources agree very well. The transition dipole moment is found to increase to larger internuclear distances. However, beyond 7 Å the change in the electronic configuration becomes obvious through substantial changes in magnitude of the transition dipole moment.

During the study of the ground state of NaRb, done in Hannover by Fourier-transform spectroscopy (FTS) of laser induced fluorescence (LIF) [10], it turned out, that a lot of information about the excited C$^1\Sigma^+$ and D$^1\Pi$ [11] states was available from the recorded spectra. For the

* Four supplementary tables (Tabs. I–IV) are only available in electronic form at `http://www.eurphysj.org`

[a] e-mail: `knoeckel@iqo.uni-hannover.de`

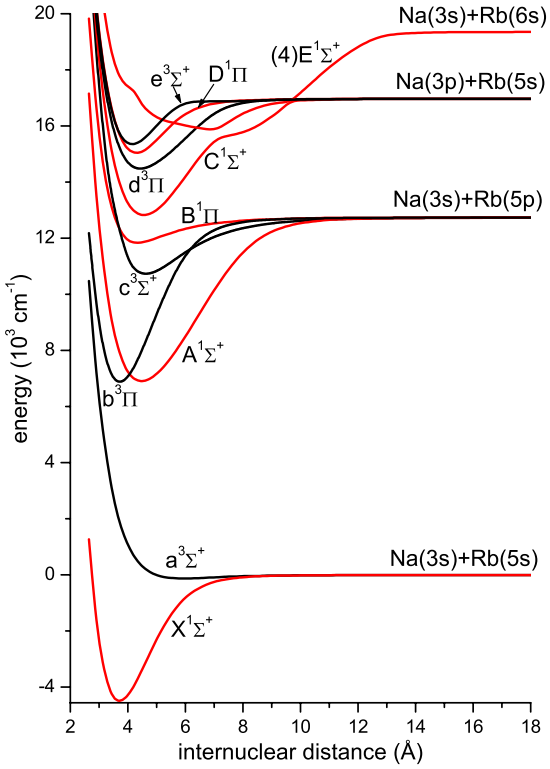

Fig. 1. Ab initio potential energy curves of the lowest Σ and Π states of NaRb according to reference [7].

C state a significant portion of the middle part of the potential energy curve (PEC) could be constructed from the FTS data, but the vibrational assignment was established from the isotope shift between $Na^{85}Rb$ and $Na^{87}Rb$ of fairly high v' only and needed confirmation. Also the bottom of the C state was still uncertain, since the main body of measurements started at a level preliminarily assigned as $v' = 21$ (later confirmed) and contained a single measurement extrapolated to be $v' = 5$. In addition, it was important to investigate the possibility for collecting experimental data on the shelf region. Moreover, in the region of low v', the C–X band overlaps with the B–X band and it would be difficult to use the LIF spectroscopy searching for $v' = 0$ of the C state since the B–X band is much more intense and in addition strongly perturbed [12]. Therefore, to enlarge and complete the data, a new experiment using the method of polarization labeling spectroscopy (PLS), which is better suited for the studies of the excited states, was performed in Warsaw. This experiment provided excitation spectra of the $C^1\Sigma^+ \leftarrow X^1\Sigma^+$ band system covering a broad range of vibrational levels in the C state, starting from $v' = 0$, in more systematic way than the FTS study (see Fig. 2 for comparison of the scope of both studies).

The experimental observations allow to derive a precise potential energy curve till up to 77% of the well depth. So it seems worthwhile to investigate through the example of the C state more deeply how the above mentioned peculiar behaviour of the transition dipole moment influences a possible production of cold NaRb molecules via photoassociation.

The paper is organized as follows. As two different experimental methods were applied at different locations, the description of the experimental part is divided into two subsections, one dedicated to the FTS experiments done in Hannover and the other to the PLS experiments in Warsaw. Then the construction of the PEC from the measurements is described, and the paper is finished by a discussion of the results and the relation to photoassociation experiments.

2 Experiments

2.1 Fourier transform spectroscopy

In the Hannover part of the experiment we studied the $C^1\Sigma^+ \rightarrow X^1\Sigma^+$ emission of NaRb. Laser induced C–X fluorescence spectra were recorded with the Bruker IFS 120 HR Fourier transform spectrometer. The experimental set-up has been described in more detail in our recent paper [10], thus we review only some essential points. The NaRb molecules were produced in a single section heat-pipe oven similar to that described in reference [13] by heating 5 g of Na (purity 99.95%) and 10 g of Rb (purity 99.75%, natural isotopic composition) from Alfa Aesar. The oven was operated at temperatures between 560 K and 600 K and typically with 2 mbar of Ar as a buffer gas. At these conditions apart from the atomic vapors all three types of molecules are formed — Na_2, Rb_2 and NaRb. Operating at relatively low temperatures we avoided strong Na_2 transitions (which became significant at higher temperatures). Rb_2 molecules were not excited with the laser lines used in this study, whereas Rb_2 fluorescence was observed when exciting with Ar^+ lines of wavelength smaller than 496.5 nm (see also Ref. [14]).

The mixture was successively illuminated by several laser sources [10]. A single mode, frequency doubled Nd:YAG laser with a typical output power of 70 mW at 532.2 nm excites transitions of the $C^1\Sigma^+ \leftarrow X^1\Sigma^+$ and $D^1\Pi \leftarrow X^1\Sigma^+$ systems of NaRb. Its frequency was varied between 18787.25 cm^{-1} and 18788.44 cm^{-1} giving rise to 18 C–X progressions. The range of v' covered in the $C^1\Sigma^+$ state by the Nd:YAG laser is $v' = 21-30$. The Ar^+ ion laser line at 514.5 nm also efficiently excites transitions in the $C^1\Sigma^+ \leftarrow X^1\Sigma^+$ system along with the excitation of transitions of the $D^1\Pi \leftarrow X^1\Sigma^+$ system. Here a range of $v' = 32-44$ in the $C^1\Sigma^+$ state was obtained. Overall, 12 progressions were assigned. It is worthwhile to mention that the Ar^+ ion laser line 501.7 nm excites $C^1\Sigma^+ \leftarrow X^1\Sigma^+$ transitions in NaRb, however due to small Franck-Condon factors the resulting fluorescence is very weak and we were only able to observe it at higher temperatures (620 K). The identified progression originates from $v' = 46$. A term value for $v' = 5$ was obtained from a weak $C^1\Sigma^+ \rightarrow X^1\Sigma^+$ LIF spectrum excited by a Rhodamine 6G dye laser. A list of the various transitions used for excitation is provided in the *Supplementary Online Material* (Tab. I) to this paper.

Due to the presence of argon buffer gas and the very good signal-to-noise ratio several strong fluorescence lines were accompanied by a large number of collisionally induced rotational satellites with ΔJ up to ± 12. The analysis of these satellites has increased the Fourier data set for the $C^1\Sigma^+$ state significantly. It also allowed us to establish a relative vibrational numbering of the levels of the $C^1\Sigma^+$ state at the early stage of analysis. Overall, from the analysis of the FTS spectra we obtained 204 term values of the NaRb $C^1\Sigma^+$ state with undoubtedly assigned isotopomer and rotational quantum numbers by using the eigenenergies of the ground state potential from reference [10]. Due to the Doppler broadening of the absorption lines, the frequencies of the fluorescence progressions excited by a single mode laser and observed in the opposite direction to the beam propagation can be shifted with respect to those of zero velocity molecules. These shifts will appear as a systematic error when calculating C-state term energies. Therefore, the uncertainty of the calculated term energies was estimated to about 0.01 cm^{-1}, i.e. larger than the relative uncertainty of the transition frequencies (0.003 cm^{-1}) used in reference [10] for determination of the ground state potential.

2.2 Polarization labeling spectroscopy

In the Warsaw part of the experiment, we studied the $C^1\Sigma^+ \leftarrow X^1\Sigma^+$ excitation spectrum of NaRb by the V-type optical-optical double resonance polarization labeling spectroscopy (V-type PLS) with two independent pump and probe lasers [15]. In our version of the method, we use a linearly polarized, weak probe laser, the fixed frequency of which is in resonance with a set of known rovibronic transitions $D^1\Pi(v', J') \leftarrow X^1\Sigma^+(v'', J'')$ in the NaRb molecule. The ground state levels (v'', J'') involved in the transitions are commonly described as 'labeled' by the probe laser. The circularly or linearly polarized, strong pump laser light is tuned across the studied C–X band system. Whenever in resonance with any molecular transition $C^1\Sigma^+(v, J) \leftarrow X^1\Sigma^+(v'', J'')$ it orients or aligns the absorbing molecules in the lower (and upper) levels by optical pumping. At the wavelengths at which a transition induced by the pump beam shares the same lower level (v'', J'') with the probe transition, the probe beam changes its polarization. This is detected with a set of crossed polarizers placed in the path of the probe beam at both sides of the molecular sample. In this way the information about the C–X spectrum of NaRb (induced by the pump laser) is contained in the transmitted intensity of the probe beam. The observed spectrum, called a 'polarization labeling spectrum', is considerably simplified by the fact that it originates only from a few ground state levels with fixed and known (v'', J'') quantum numbers, whereas a broad range of vibrational levels in the C state can be sampled.

In the experiment the NaRb molecules (natural isotopic composition) were prepared by heating about 1 cm^3 of metallic sodium and 1 cm^3 of rubidium in a stainless steel heat pipe with a heated zone 20 cm long. The temperature was maintained at approximately 650 K and a total pressure of 5 mbar was established using argon as a buffer gas. As the polarization measurements were carried out at significantly higher working temperature than those in Hannover, after several hours of operation, the metals tended to separate and rubidium condensed in cold parts of the pipe, close to the water cooling zones. Therefore, the oven had to be refreshed approximately every 6 hours by heating the condensation zones to restore the rubidium metal to the central part of the oven. With this procedure the measurements were completed without refilling the heat pipe with fresh metals.

The copropagating pump and probe laser beams were crossed at the center of the heat pipe. The probe laser was kept at fixed wavelength (multimode Ar^+ laser operating at 476.5, 488.0, 496.5, 501.7 or 514.5 nm) exciting transitions in the $D^1\Pi \leftarrow X^1\Sigma^+$ band system of NaRb known from the previous experiment [10]. This ensured labeling of known rovibrational levels of the ground state. However, for some of the Ar^+ laser wavelengths, high congestion of lines in the D–X system resulted in simultaneous labeling of several levels. To decrease the number of them, in order to further simplify the recorded spectra, the probe laser could also be run in a single mode regime, using an intracavity etalon. In this case the single mode frequency was adjusted by tilting the etalon, to optimize labeling of a desired ground state level.

The pump laser (pulsed dye laser with XeCl excimer laser as pump, 2 mJ pulse energy, 0.1 cm^{-1} spectral width) was tuned across the $C^1\Sigma^+ \leftarrow X^1\Sigma^+$ band system under investigation, in the spectral range 16850–20300 cm^{-1}. Beyond 20300 cm^{-1} no further lines could be observed. The pump laser frequency was calibrated against the optogalvanic spectrum of argon and frequency markers were provided by a 0.5 cm long Fabry-Perot interferometer. The absolute accuracy of the measured positions of the spectral lines was estimated conservatively to be 0.05 cm^{-1}. The uncertainty was increased for weaker or overlapped lines. In order to convert the transition frequencies to energy levels of the $C^1\Sigma^+$ state we used the accurate data on the $X^1\Sigma^+$ state levels from reference [10]. When information on given level came from several transitions a weighted average was used for its term value. Due to high sensitivity of the experimental method, by recording the molecular spectra almost background free, we were able to measure positions even of very weak lines in the C–X band system. For vibrational progressions which are expected to be particularly long because of favorable Franck-Condon factors, the pump laser power was chosen individually for the different strengths of specific parts of the spectra, and the probe laser was used in a single mode tuned to a frequency giving a maximum polarization signal. As a result, our PLS data correspond to a broad range of vibrational levels in the $C^1\Sigma^+$ state, $v' = 0{-}64$.

The whole data field available from both measurements is shown in Figure 2. All observations are published in the *Supplementary Online Material* (Tab. II) to this paper.

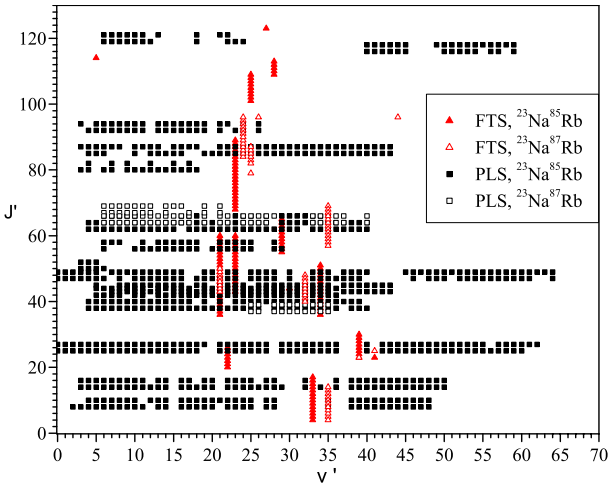

Fig. 2. Distribution and sources of the experimental data used in the analysis of the $C^1\Sigma^+$ state of NaRb, accuracy of FTS data 0.01 cm^{-1}, of PLS data 0.05 cm^{-1}.

3 Data analysis and reduction to a potential

In the analysis of the LIF FTS experimental data rotational quantum numbers were assigned from the splitting of P–R doublets as the ground state potential is well-known [10]. Relative vibrational numbering was established from v', J' term values plotted against $J'(J'+1)$. An initial absolute numbering was based on the ab initio curves calculated in reference [7].

In order to improve the reliability of the theoretical calculations, however, we decided not to use directly the calculated potentials from reference [7]. Following the idea of reference [8], first the difference between the ground state and the C state ab initio potentials was calculated and then the result was added to the experimental potential of the X state of reference [10], $U(\mathrm{C})_{dif} = U(\mathrm{X})_{exp} + (U(\mathrm{C})_{ab\ initio} - U(\mathrm{X})_{ab\ initio})$. The basic idea shared with reference [8] is that approximations in the ab initio calculations may influence different electronic states in the same direction. Therefore, usually the accuracy of the difference between two ab initio PEC is expected to be higher than the quality of the individual potentials. Although this was stated for a specific ab initio approach in reference [8], here we applied a similar procedure to the calculations of reference [7] and found that it gives quite good results.

Due to the special shape of the potential energy curve of the C state we decided to apply the fitting routine from reference [16] based on the Inverted Perturbation Approach (IPA) and originally suggested and developed in references [17,18]. Contrary to the first implementations of the IPA method, the code from reference [16] turned out to be very successful when applied not only to regular potentials (e.g. [10]) but also to a variety of potentials of exotic shapes like double minimum potentials [19], curves with "shelf" regions [20,21] and others [22,23]. A key point is the representation of the potential as a set of grid points connected with a cubic spline function over the range of internuclear distances covered by experimental data. To larger distances a long range extension $U_{LR} = D_e - C_6/R^6 - C_8/R^8 - C_{10}/R^{10}$ was used, with C_6 and C_8 taken from [24] and C_{10} adjusted to give a smooth transition between the pointwise and the long range part. D_e is the dissociation asymptote referred to the minimum of the ground state. The advantages of this presentation are its flexibility and a moderate correlation between the fitted parameters (i.e. ordinates of the grid points). The flexibility, however, can often result in unphysical oscillations of the fitted potential curve. This happens usually in the regions which are not sufficiently described by the experimental data. To handle the problem the Singular Value Decomposition [25] is used for minimization of the merit function $\chi^2(U)$. Very recently [26] an additional tool was suggested — a regularization functional added to the merit function which is responsible for the smoothness of the solution. Since the realization of the IPA fitting routine with pointwise representation of the potential was described in references [16,26,20–23] and the application of a regularizing functional is straightforward (see e.g. Ref. [26]), we will skip the details about it and pass directly to the fit of the PEC of the C state.

The start guess for the PEC was the difference based theoretical potential $U(\mathrm{C})_{dif}$ as described at the beginning of the section, and was defined in an equidistant grid of 33 points between $R = 2.65$ Å and 12.7 Å. With only few iterations of the IPA routine it was possible to fit all the LIF data for both NaRb isotopomers with a single PEC. This was considered as a first indication that the vibrational numbering suggested by the difference-based theoretical potential is correct. Since the FTS data set had quite a limited range of vibrational quantum numbers (from 21 to 46), we tested the vibrational assignment by constructing new potentials assuming a vibrational shift of $\Delta v = +1$ and $\Delta v = -1$. As we expected, the attempts to fit the experimental results of both $Na^{85}Rb$ and $Na^{87}Rb$ with a single potential within the experimental uncertainty failed in these cases. An additional test was made by a comparison of the calculated Franck-Condon factors (FCF) of the C–X transitions with the experimental intensity distributions of LIF. It appeared that only the potential with the initially assumed vibrational assignment was able to give FCF reproducing the observations.

For a satisfactory description of the whole C state, however, more data were needed. The first goal was to fix the bottom of the C state, by including transitions to/from levels of the C state down to $v' = 0$. Additionally, levels with high vibrational quantum numbers were desirable in order to describe the "shelf" region of the C state. Due to overlaps of the C–X band with the perturbed B–X band in the region of low v' LIF spectroscopy was ruled out for the search for $v' = 0$, and we employed the V-type PLS using the set-up in Warsaw, as an excitation spectroscopy technique. Its high selectivity allowed us to greatly simplify the excitation spectra where, in addition to the NaRb B–X, C–X and D–X bands, the intense Na_2 A–X and B–X bands are located. Due to the tunable pulsed laser used as pump laser an extension of the C state to the shelf region of the potential curve was possible.

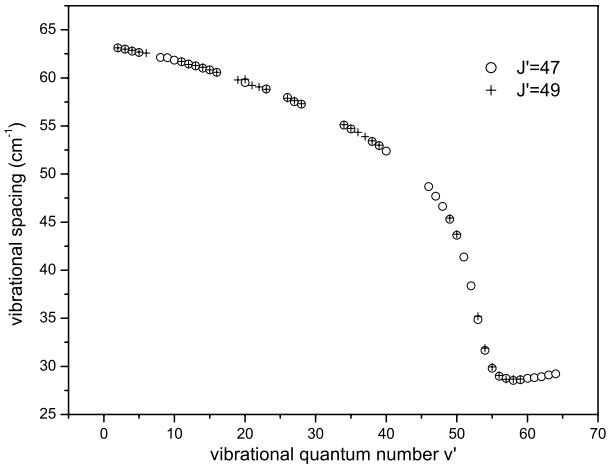

Fig. 3. Vibrational spacings of the C state as a function of vibrational quantum number v' for $J' = 47$ and $J' = 49$. The sudden drop of the level spacing on entering the shelf region for $v' > 50$ is obvious.

The preliminary potential constructed with the FTS data allowed us to unambiguously assign the C–X progressions observed with the PLS method. We selected for labeling such ground state levels from which favorable Franck-Condon factors to the bottom of the C state and to the shelf region exist. For low v' deviations of the measured and the predicted line positions, calculated with the preliminary C-state potential and the X state potential [10] reached up to few wavenumbers for $v' = 0-2$.

The C state potential was gradually improved as new data with lower v' were included. As transitions to the lowest v' of the C state coincide with the much stronger B–X transitions, in order to be sure that the assigned lines belong to the C–X band we performed several measurements with a single mode probe laser. By changing slightly the frequency of the probe laser and observing the change of the line intensities we convinced ourselves that the suspected transitions to the lowest v' of the C state change their intensities in the same way as the transitions to higher v' of the same progression where the assignment was without doubt. In this way accidental coincidences with other molecular transitions were excluded.

Once the bottom of the C state was fixed, we tuned the pump laser to the region 19500−20300 cm^{-1} looking for transitions to high v' levels in the shelf. Again the potential was gradually re-fitted each time new experimental data were recorded. This was especially necessary when the shelf region was approached, since there the vibrational spacing starts to decrease much faster than in typical anharmonic potentials. Here we could take full advantage of the flexibility of our data reduction method, whereas the use of molecular constants like Dunham parameters became almost impossible. As an example the behavior of the vibrational energy spacing is shown in Figure 3 for the longest recorded vibrational progression, reaching $v' = 64$ with $J' = 47$ and 49. The onset of the shelf region is clearly visible due to the bend in the curve for $v' > 50$. Although the probe laser was used in single mode operation, we failed to follow the labeled C–X progressions beyond $v' = 64$ for Franck-Condon reasons and due to the presence of the much stronger NaRb D–X and the Na_2 B–X systems.

Table 1. List of potential energy grid points for the C(3)$^1\Sigma^+$ state. The full data set is represented with a standard deviation of 0.037 cm^{-1}. The dissociation asymptote D_e refers to the minimum of the ground state, beyond R_O the long range expansion is used, see text.

R (Å)	$U(R)$ (cm^{-1})	R (Å)	$U(R)$ (cm^{-1})
2.6000	27339.156	5.7188	18627.109
2.7190	25761.642	5.8799	18856.610
2.8380	24277.932	6.0410	19091.257
2.9570	22970.966	6.2020	19326.105
3.0760	21903.509	6.3631	19557.231
3.1950	21024.166	6.5241	19780.173
3.3140	20270.612	6.6852	19990.929
3.4330	19631.429	6.8462	20183.582
3.5519	19105.284	7.0073	20350.560
3.6709	18678.278	7.2342	20519.818
3.7899	18338.747	7.4612	20608.871
3.9089	18075.017	7.6881	20666.835
4.0278	17876.402	7.9151	20728.386
4.1468	17733.865	8.1420	20807.328
4.2658	17639.271	8.5707	21017.979
4.3848	17585.876	8.9993	21330.484
4.5038	17568.111	9.4280	21740.865
4.6228	17581.281	9.8567	21910.956
4.7418	17621.977	10.2853	21950.712
4.8815	17699.640	10.7140	21968.140
5.0209	17805.681	11.1427	21976.325
5.1605	17936.028	11.5700	21980.261
5.3001	18086.687	12.0000	21982.330
5.4397	18254.406	12.4300	21983.475
5.5793	18435.788		
D_e	21986.672 cm^{-1}	R_O	12.11009 Å
C_6	-2.429×10^6 Å^6 cm^{-1}	C_8	2.1416×10^9 Å^8 cm^{-1}
C_{10}	9.36942×10^9 Å^{10} cm^{-1}		

The final potential describes the experimental term energies of both $Na^{85}Rb$ (1001 levels) and $Na^{87}Rb$ (160 levels) isotopomers. The relatively small number of $Na^{87}Rb$ transitions is due to the fact that most of the experimental data were collected by PLS, where suitable transitions labeled by the Ar^+ laser are mainly in $Na^{85}Rb$. The potential is defined at 49 points and is listed in Table 1. In order to interpolate between the grid points a natural cubic spline [25] is used (i.e. the second derivatives in the first and the last grid points are set to zero). The potential reproduces the PLS data with a standard deviation of 0.037 cm^{-1} and a dimensionless standard deviation of 0.79. The LIF data are reproduced with a standard deviation of 0.0083 cm^{-1} and a dimensionless standard deviation of 0.83. The combined dimensionless standard deviation for both data sets amounts to 0.80. For a conventional spectroscopic use a list of Dunham coefficients

Table 2. Dunham parameters for the $C(3)^1\Sigma^+$ state of $Na^{85}Rb$ for the limited range $0 \leq v' \leq 40$ and $8 \leq J' \leq 121$. $T_e + Y_{00}$ is referred to the minimum of the ground state potential. The limited data set is represented with a standard deviation of 0.02 cm^{-1}.

parameter	value (cm^{-1})	uncertainty (cm^{-1})
$(T_e + Y_{00})_{\mathrm{Dun}}$	0.17568128×10^5	0.12×10^{-1}
Y_{10}	0.636019×10^2	0.44×10^{-2}
Y_{20}	-0.4156×10^{-1}	0.57×10^{-3}
Y_{30}	-0.22266×10^{-2}	0.33×10^{-4}
Y_{40}	0.30505×10^{-4}	0.86×10^{-6}
Y_{50}	-0.3383×10^{-6}	0.82×10^{-8}
Y_{01}	0.4579804×10^{-1}	0.50×10^{-5}
Y_{11}	-0.13316×10^{-3}	0.11×10^{-5}
Y_{21}	-0.1195×10^{-5}	0.89×10^{-7}
Y_{31}	0.4089×10^{-7}	0.28×10^{-8}
Y_{41}	-0.8097×10^{-9}	0.32×10^{-10}
Y_{02}	-0.91916×10^{-7}	0.28×10^{-9}
Y_{12}	0.9417×10^{-9}	0.29×10^{-10}
Y_{22}	-0.2788×10^{-10}	0.70×10^{-12}

for the C state of $Na^{85}Rb$ is given in Table 2. They reproduce the experimental term energies in the range $0 \leq v' \leq 40$ and $8 \leq J' \leq 121$ with a dimensionless standard deviation of 0.92. Including the levels of the shelf region for an entire description of the data by the Dunham formalism would be unreasonable due to an enormously large number of parameters necessary. The potential data and the Dunham parameters are also given in the *Supplementary Online Material* (Tabs. III and IV) to this paper.

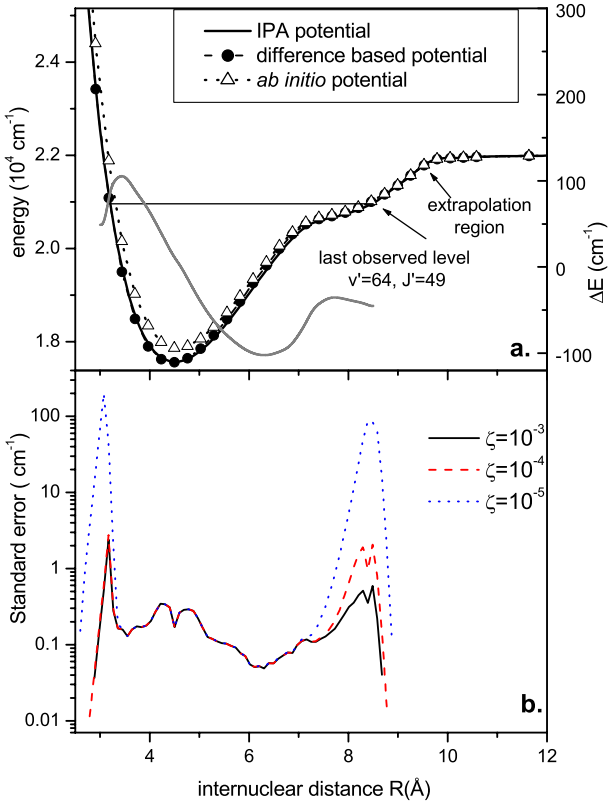

Fig. 4. (a) Comparison of the experimental IPA potential for the $C^1\Sigma^+$ state (solid line) and the corresponding ab initio potential by Korek et al. [7] (triangles and dotted line) and the difference based potential $U(C)_{dif} = U(X)_{exp} + (U(C)_{ab\ initio} - U(X)_{ab\ initio})$ (full circles), see text. In grey: $\Delta E = U(C)_{exp} - U(C)_{dif}$, referred to the right hand scale. (b) Standard error of the fitted parameters for three different values of the singularity parameter ζ.

4 Discussion

The present measurements characterize 77% of the C-state potential well depth from the bottom (U_{min} = 17568.07 cm^{-1}) up to about 21000 cm^{-1} (see Fig. 4), which is still about 1000 cm^{-1} below the Na $3p\ ^2P_{1/2}$ + Rb $5s\ ^2S_{1/2}$ asymptote. The last observed rovibronic level is located well in the shelf region. In Figure 4a the experimental potential is compared to the ab initio potential from reference [7] (triangles in Fig. 4a) and the difference based potential (full circles).

As one can see, the difference-based potential is much closer to the experimental one than the ab initio potential, so that the statement from reference [8] is confirmed here. The grey line in Figure 4a displays the magnified difference $\Delta E = U(C)_{exp} - U(C)_{dif}$, referring to the right hand scale for better visibility, and shows variations of about 100 cm^{-1}, whereas the difference between the experimental and the ab initio potentials is as large as 300 cm^{-1} at the potential minimum and up to 600 cm^{-1} in the short range part. This finding suggests that for comparison with experimental results it is better to use the differences of ab initio potential curves.

Some caution has to be applied to the uncertainties of the Dunham parameters given in Table 2 and especially for that of T_e. During the fitting procedure for the potential energy curve we observed that the potential minimum is determined with relatively large ambiguity. U_{min} varied from fit to fit, depending on the number of fitted parameters to within ± 0.2 cm^{-1}. Analysis of the uncertainties of the potential, similar to that from references [20,21] confirmed such a level of uncertainty of the potential minimum. In Figure 4b the standard error of the fitted parameters is shown for three different values of the singularity parameter ζ used within the Singular Value Decomposition technique in order to avoid changes in the potential shape not caused by the experimental data. Regions where the standard error does not change with ζ are fixed mainly by the experimental data (see Refs. [20,21] for a detailed discussion). Outside these regions the variation of the potential is limited by ζ and therefore its shape is less well described within the present data set. In this respect, the potential minimum is well determined by the data and the standard error read off from the fit should be significant, it reaches 0.3 cm^{-1} there. On the other hand the value of T_e determined from the Dunham coefficients (with $Y_{00} = 0.022$ cm^{-1} for the C state) was not so sensitive to the number of Dunham coefficients and the range of the

experimental data and stays always around the value reported in Table 2. In principle T_e should agree with U_{min}. However, a small difference remains, but well within the expected uncertainty of U_{min}. Presently, we attribute the large difference in the estimation of the uncertainty to the kind of flexibility of both representations: the small uncertainty in T_e in the fit of Dunham coefficients originates from the rigidness of this model, whereas the larger uncertainty in U_{min} is due to the small amount of experimental data near the potential minimum and the flexibility of the pointwise representation of the potential. We would like to stress here the intrinsic uncertainty in the determination of the potential minimum, which is only indirectly defined by the experimental data and is model dependent, especially when extrapolated from a scarce data set.

With the potentials for the X ground state and the C state now available the question can be addressed, if the C state could be a well suited intermediate state for photoassociation of cold NaRb ground state molecules.

The discussion should be taken as a qualitative guide. It will be restricted to the hypothetical case, that photoassociation takes place exclusively in the singlet system, and we shall give an estimation only, because the hyperfine structure and the singlet-triplet mixing at the ground state asymptote due to hyperfine interaction is neglected. The C state branching by coupling to the E state is also not taken into account, compare Figure 1.

The shelf of the C state appears due to an ion-pair state crossing the covalent states and giving rise to avoided crossings [7]. This can be seen in Figure 1. Because the electronic configuration will change from covalent to ionic and back, a change in the transition dipole moment for the C–X transitions is expected.

In fact, the transition dipole moment function $D(R)$ calculated by Aymar and Dulieu [9] shows quite peculiar behaviour. Starting at about 2.1 Å with $0.8ea_0$ (e elementary charge, a_0 Bohr radius), $D(R)$ increases until 7.5 Å to $2.4ea_0$, then drops sharply to about $0.8ea_0$ at about 9 Å as a consequence of the change to the ion-pair configuration at the first avoided crossing. Then it rises sharply again to a value of $2.2ea_0$ due to the transition back to a covalent configuration at about 10 Å. To larger internuclear distances it increases to the separated atoms value. Thus the C–X dipole moment function is everywhere different from zero and does not change its sign, but has a substantially smaller value in the shelf region, where the ion-pair configuration prevails.

We used this function of the transition dipole moment to calculate the transition matrix elements of interest. To work out the influence of this dip on the transition moments, we have also used a second "modified" dipole moment function, which has been set to the atomic value for $R > 7$ Å, for comparison with the "true" one.

For the wavefunctions of the ground state we used a refined version of the potential published in reference [10], which supports 81 vibrational levels for $J = 0$. Refinement of the potential was necessary because recently higher ground state vibrational levels up to $v'' = 78$ were observed experimentally (a report is in progress [27]) while the last observed vibrational level in reference [10] was $v'' = 76$.

The potential of the C state given in Table 1 supports 103 bound vibrational levels. It must be emphasized that its part with internuclear distances greater than 9 Å is only poorly defined experimentally and is based mainly on ab initio calculations. Note also a potential barrier, due to the sign of C_6, of 2×10^{-3} cm^{-1} height at $R \approx 31$ Å for $J = 0$.

We assume s-wave scattering and start with a continuum wavefunction $\langle E_{cont}, l = 0|$ about 140 μK above the ground state asymptote and rotational quantum number $l = 0$. We calculate the transition matrix element $\langle E_{cont}, 0|D(R)|v_C, 1\rangle$ to the vibrational level v_C and rotational quantum number $J = 1$ of the C state. The wavefunction of the ground state is calculated using the Numerov algorithm and normalization to Bessel functions at large interatomic separation. This gives a dipole matrix element which can be used to estimate the rate of photoassociation of bound C state molecules from the low kinetic energy ground state continuum. The largest matrix elements actually occur for transitions to levels close to the C-state asymptote, for v_C between 97 and 101. Assuming conditions of cold collisions ($T = 140$ μK, $n = 10^{17}$ m^{-3}, laser power 10^7 Wm^{-2}), formula (1) of [6] (with average angular factor $A_\Omega = 0.01$ according to Tab. 1 of Ref. [28]) yields PA rates of maximum 300 s^{-1} for $v_C = 100$. However, also around $v_C = 61$ (an observed level) rates only about a factor of 10 smaller occur. The former can be excited with a laser at 16944.61 cm^{-1} (590.0 nm in air), which is red detuned by 11.56 cm^{-1} with respect to the asymptote Na $3p\ ^2\mathrm{P}_{1/2}$+Rb $5s\ ^2\mathrm{S}_{1/2}$ at 21986.672 cm^{-1}, while the latter requires an excitation at 15804.627 cm^{-1} (632.5 nm in air). The rates decrease to essentially zero for $v_C \leq 34$. The nonzero rates at fairly low v_C are due to shape and relative internuclear distance of X and C state and originate from overlap of the parts of the wavefunctions in the bound region of the ground state. The above statements remain essentially also valid when using the second "modified" dipole moment function. Only in the interval $67 \leq v_C \leq 93$ it yields rates larger by a factor of about 3 compared to the true dipole moment function.

The largest rates found here for the X–C transition are smaller by about two orders of magnitude when compared to the results for the NaRb $\mathrm{X}^1\Sigma^+$–$\mathrm{A}^1\Sigma^+$ transition [6]. This gives indeed preference to the choice of the A state for PA experiments.

As examples PA rates and additional information for a set of high levels in $\mathrm{C}^1\Sigma^+$ are given in Table 3. The second column gives the outer turning radius R_O of vibrational motion, the third the red detuning of the upper levels v_C from the asymptote, and the fourth column gives the calculated PA rates.

We also derived the probability distribution of population $P(v_X)$ in the final levels of the ground state by spontaneous decay. It is given by the Einstein A-factors $A(v_C,v_X)$ out of the excited level v_C to the final ground

Table 3. Photoassociation rates and calculated relative population distribution from decay of upper PA level v_C to ground state levels v_X. For assumed experimental conditions see text. R_O denotes the classical outer turning point for v_C. The third column gives the calculated energy differences of the levels v_C with respect to the asymptote Na $3p\ ^2\mathrm{P}_{1/2}$ + Rb $5s\ ^2\mathrm{S}_{1/2}$ at 21986.672 cm^{-1}. PA rates and branching ratios were calculated following reference [6]. Only values above 0.001 are given.

v_C	R_{out}(Å)	red detuning (cm^{-1})	PA rate (s^{-1})	branching ratio	$P(v_X)$						
					$v_X = 6$	7	8	9	69	70	72
61	8.210	1151.543	34	0.459	0.010	0.019	0.023	0.014	0.086	0.189	0.175
					$v_X = 74$	75	76	77	78	79	80
96	9.834	79.8348	26	0.287	0.458	0.150	0.129	0.010	0.002	0.006	0.005
97	9.996	56.6819	80	0.160	0.367	0.354	0.078	0.002	0.021	0.020	0.010
98	10.255	37.5059	95	0.266	0.207	0.528	0.005	0.095	0.067	0.029	0.011
99	10.585	22.8075	26	0.154	0.022	0.456	0.339	0.138	0.011		0.001
100	11.050	11.5617	314	0.202	0.002	0.099	0.672	0.029	0.097	0.058	0.024
101	11.890	4.7354	167	0.047		0.004	0.211	0.761	0.002	0.007	0.007
102	13.477	1.6005	34	0.023				0.159	0.837	0.001	0.001

state levels $|v_X, 0\rangle$, normalized to unity,

$$P(v_X) = \frac{A(v_C, v_X)}{\sum_{v_X=0}^{80} A(v_C, v_X)}. \quad (1)$$

For true rates of cold molecule production, they have to be multiplied with the branching ratio of the transition probability to bound levels in the X state and the total transition probability. For the calculation we follow the reasoning of reference [6], summing the Franck-Condon factors from the upper state to all lower bound ones. Examples are given in the fifth column of Table 3. The calculation yields largest population for final states $74 \leq v_X \leq 80$. The changes from one v_X to the next one are mainly due to changes in the outer turning points of the X state, which are much larger than for the C state. Obviously, choosing $v_C = 101$, the mostly populated final levels will be $v_X = 76$ and 77 with a yield of 15% for 77. Exciting $v_C = 61$, the population will be distributed from $v_X = 68$ to 78, with maxima of about 9% for 70 and 72, but also about 0.5% will end in $v_X = 6$ to 8. The total rate of formation of cold molecules in a specific final level of the ground state can be taken from Table 3 as the product of PA rate, branching ratio and relative probability distribution $P(v_X)$, because the decay rate is high compared to the PA rate.

Applying the second "modified" dipole moment function in these calculations, the above statements remain valid. Changes by factors of about 3 are observed here for rates from $v_C = 67$ to 93 to $v_X = 70$ to 78. Thus the change in transition moment due to the configuration change from covalent to ionic in the shelf part of the potential and back to covalent at the asymptote appears through moderate changes in transition rates for states, which are located in the shelf region. This behaviour also restricts the range of favourable upper PA levels to only few close to the asymptote.

The Warsaw team gratefully acknowledges partial support received from the Polish Committee for Scientific Research (KBN grant number 2 P03B 063 23). The work is supported by DFG through SFB 407, and by the EC network "Cold Molecules" (Contract No. HPRN-CT-2002-00290). O.D., M.T. and R.F. acknowledge funding by the NATO SfP 978029 grant and by the EC 5th Frame "Competitive and Sustainable Growth" Grant G1MA-CT-2002-04063 as well as by Latvian Science Council grant No. 04.1308 and Latvian Government Grant ES 03-40. A.P. acknowledges a support from the Alexander von Humboldt Foundation and Center of Excellence ASPECT (program "Competitive and Sustainable Growth", G6MA-CT-2002-04021).

References

1. For an overview of the present activitities in the field of ultracold molecules, see special issue Eur. Phys. J. D **31**, No. 2 (2004)
2. D. Wang, J. Qi, M.F. Stone, O. Nikolayeva, B. Hattaway, S.D. Gensemer, H. Wang, W.T. Zemke, P.L. Gould, E.E. Eyler, W.C. Stwalley, Eur. Phys. J. D **31**, 165 (2004)
3. T. Bergeman, A.J. Kerman, J.M. Sage, S. Sainis, D. DeMille, Eur. Phys. J. D **31**, 179 (2004)
4. C. Haimberger, J. Kleinert, M. Bhattacharya, N.P. Bigelow, Phys. Rev. A **70**, 21402 (2004)
5. M.W. Mancini, G.D. Telles, A.R.L. Caires, V.S. Bagnato, L.G. Marcassa, Phys. Rev. Lett. **92**, 133203 (2004)
6. S. Azizi, M. Aymar, O. Dulieu, Eur. Phys. J. D **31**, 195 (2004)
7. M. Korek, A.R. Allouche, M. Kobeissi, A. Chaalan, M. Dagher, K. Fakherddin, M. Aubert-Frécon, Chem. Phys. **256**, 1 (2000)
8. A. Zaitsevskii, S.O. Adamson, E.A. Pazyuk, A.V. Stolyarov, O. Nikolayeva, O. Docenko, I. Klincare, M. Auzinsh, M. Tamanis, R. Ferber, R. Cimiraglia, Phys. Rev. A **63**, 052504 (2001)
9. M. Aymar, O. Dulieu, private communication (2004)
10. O. Docenko, M. Tamanis, R. Ferber, A. Pashov, H. Knöckel, E. Tiemann, Phys. Rev. A **69**, 042503 (2004)
11. O. Docenko, M. Tamanis, R. Ferber, A. Pashov, H. Knöckel, E. Tiemann, Eur. Phys. J. D (2005, submitted)

12. Y.-C. Wang, K. Matsubara, H. Katô, J. Chem. Phys. **97**, 811 (1992)
13. O. Allard, C. Samuelis, A. Pashov, H. Knöckel, E. Tiemann, Eur. Phys. J. D **26**, 155 (2003)
14. C. Amiot, J. Chem. Phys. **93**, 8591 (1990)
15. W. Jastrzebski, P. Kowalczyk, Phys. Rev. A **51**, 1046 (1995)
16. A. Pashov, W. Jastrzebski, P. Kowalczyk, Comput. Phys. Commun. **128**, 622 (2000)
17. W. Kosman, J. Hinze, J. Mol. Spectrosc. **56**, 93 (1975)
18. C. Vidal, H. Scheingraber, J. Mol. Spectrosc. **65**, 46 (1977)
19. W. Jastrzebski, W. Jasniecki, P. Kowalczyk, R. Nadyak, A. Pashov, Phys. Rev. A **62**, 042509 (2000)
20. W. Jastrzebski, A. Pashov, P. Kowalczyk, J. Chem. Phys. **114**, 10725 (2001)
21. A. Pashov, W. Jastrzebski, P. Kowalczyk, J. Chem. Phys. **113**, 6624 (2000)
22. W. Jastrzebski, R. Nadyak, P. Kowalczyk, Chem. Phys. Lett. **374**, 297 (2003)
23. A. Grochola, W. Jastrzebski, P. Kowalczyk, S. Magnier, M. Aubert-Frécon, J. Mol. Spectrosc. **224**, 151 (2004)
24. B. Bussery, Y. Achkar, M. Aubert-Frećon, Chem. Phys. **116**, 319 (1987)
25. W.H. Press, S.A. Teukolski, W.T. Vetterling, B.P. Flannery, *Numerical Recipes in Fortran 77* (Cambrige Unversity Press, 1992)
26. A. Grochola, W. Jastrzebski, P. Kowalczyk, A. Pashov, J. Chem. Phys. **121**, 5754 (2004)
27. A. Pashov, O. Docenko, M. Tamanis, R. Ferber, H. Knöckel, E. Tiemann, Phys. Rev. A (2005, submitted)
28. C. Drag, B. Laburthe Tolra, O. Dulieu, D. Comparat, M. Vatasescu, S. Boussen, S. Guibal, A. Crubellier, P. Pillet, IEEE J. Quant. El. **36**, 1378 (2000)